Applied Catalysis B: Environmental 134–135 (2013) 1–6

Contents lists available at SciVerse ScienceDirect

Applied Catalysis B: Environmental

journal homepage: www.elsevier.com/locate/apcatb

Synthesis and characterization of Ag_3PO_4 immobilized in bentonite for the sunlight-driven degradation of Orange II

Jianfeng Ma[a,b,*], Jing Zou[a], Liangyin Li[a], Chao Yao[a], Tianli Zhang[a], Dinglong Li[a]

[a] School of Environmental and Safety Engineering, Changzhou University, Changzhou, Jiangsu, China 213164
[b] State Key Laboratory of Silicon Materials, Zhejiang University, Hangzhou, China 310027

ARTICLE INFO

Article history:
Received 5 August 2012
Received in revised form
16 December 2012
Accepted 22 December 2012
Available online 2 January 2013

Keywords:
Photocatalysis
Visible light
Silver phosphate
Wastewater treatment

ABSTRACT

A novel method for intercalating silver salt into bentonite interlayers is described. The very fine Ag_3PO_4 crystalline grains (less than 0.45 nm) were obtained in the interlayers of bentonite (Ag_3PO_4-Ben). Ag_3PO_4-Ben was characterized by XRD, FTIR, XRF, XPS and UV–vis diffuse reflectance spectroscopy. Ag_3PO_4-Ben particles exhibited high catalytic efficiency for Orange II degradation under visible light irradiation. The photocatalytic activity is attributed to the small-sized Ag_3PO_4 crystal immobilized in bentonite and the strong adsorption of dye on bentonite. The special structure of bentonite and the microenvironment around the catalysis enhanced the stability.

1. Introduction

Semiconductor-based photocatalysts have received significant attention in applications for environmental protection and solar energy conversion. Ag_3PO_4, a visible light photocatalyst, can oxidize water and decompose organic contaminants in aqueous solutions [1]. Ag_3PO_4 exhibits extremely high photocatalytic efficiency for organic dye decomposition under visible light irradiation [1–6].

The large surface area of small-sized particles is expected to be beneficial for photocatalytic reactions that mostly occur on the surface of the catalysts [7]. The particle size of silver orthophosphate shows an obvious effect on the degradation of dyes. Dinh et al. [2] synthesized silver orthophosphate nanocrystals in the range of 8–16 nm that demonstrated superior photocatalytic activity under visible light compared with micron-sized Ag_3PO_4 particles. However, the nanoparticles aggregated quickly into micrometer-sized particles in aqueous solutions, thus hindering their practical applications.

As the particle size decreases to nanoscale, it is difficult to separate them from the reaction systems. To immobilize them on appropriate supports is beneficial for wastewater treatment by nanocatalysts. Cui et al. [4] demonstrated that small-sized and well-distributed Ag_3PO_4 particles immobilized on flaky layered double hydroxide (FLDH) together with the strong adsorption of dye enhanced its photocatalytic properties. The average diameter of well-distributed Ag_3PO_4 particles in the Ag_3PO_4/FLDH composite was about 200 nm. It could enhance the photocatalytic activity by continuously decrease the particle size. However, the way to reduce the crystallite size of Ag_3PO_4 smaller than 1 nm and its effect on photocatalysis is unknown.

Bentonite, a clay mineral which is abundant on the earth, consists of layers of two tetrahedral silica sheets sandwiching one octahedral alumina sheet. Bentonite is negative charged due to the isomorphic substitutions of Al^{3+} for Si^{4+} in the tetrahedral layer and Mg^{2+} for Al^{3+} in the octahedral layer. This negative charge is balanced by the presence of exchangeable cations (e.g., Na^+, Ca^{2+}, and so on) in the lattice structure, which allow excellent performance in the adsorption of cationic contaminants by cationic exchange [8,9]. For example, Ag^+ can be spontaneously adsorbed on natural bentonite and this process is spontaneous [10].

Bentonite is also a very good catalyst carrier [11,12]. Chen and Zhu [12] catalytically degraded Orange II via the ultra-violet (UV)-Fenton reaction with hydroxyl-Fe pillared bentonite in water, which overcame drawbacks such as the limited range of pH and the difficulty of separating the catalysts from the water.

However, Ag_3PO_4 is an insoluble salt. It is difficult to immobilize it between the lamellas of bentonite via cationic exchange. Some research results show that Ag^+ can be exchanged spontaneously in the inter-lamellar layer of bentonite [10,13,14]. When

* Corresponding author at: School of Environmental and Safety Engineering, Changzhou University, Changzhou, Jiangsu, China 213164. Tel.: +86 519 86330086; fax: +86 519 86330083.
E-mail address: jma@zju.edu.cn (J. Ma).

0926-3373/$ – see front matter © 2013 Elsevier B.V. All rights reserved.
http://dx.doi.org/10.1016/j.apcatb.2012.12.032

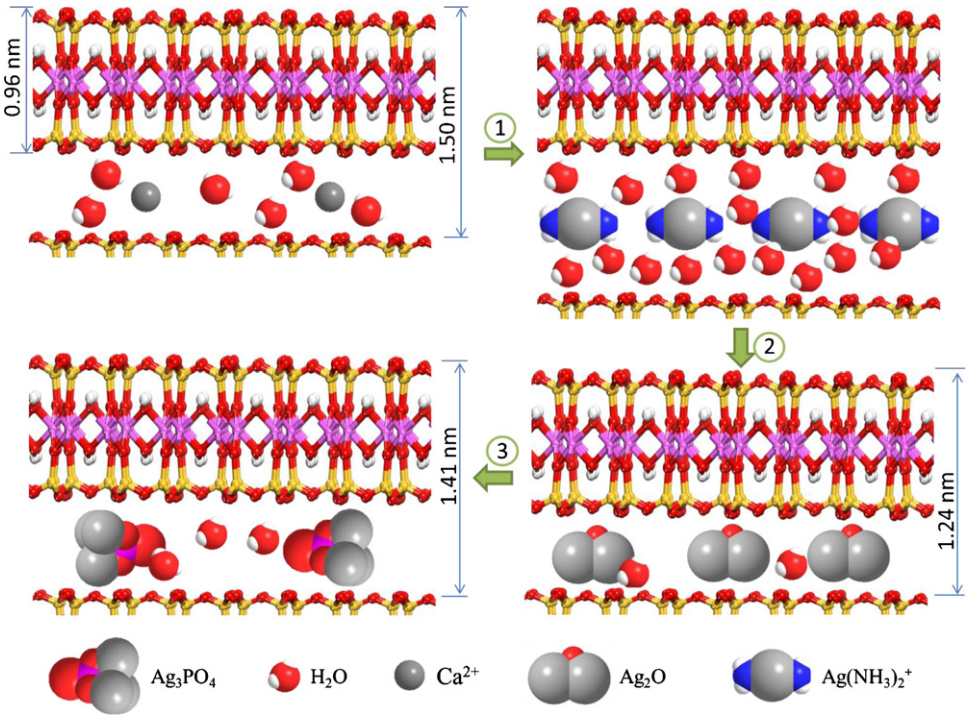

Fig. 1. Schematic illustration of the synthesis of Ag_3PO_4-Ben.

Ag^+ is exchanged into the inter-layers, the speciation of silver can be transferred to Ag_3PO_4 by react with phosphoric acid. Based on this design, we synthesized Ag_3PO_4/bentonite (Ag_3PO_4-Ben) composites. Finer Ag_3PO_4 crystalline grains were obtained between bentonite inter-layers, and the Ag_3PO_4-Ben composite exhibited higher visible light photocatalytic efficiency compared with free Ag_3PO_4 particles.

2. Experimental

2.1. Synthesis of materials

Natural bentonite, which is primarily composed of Ca^{2+}-montmorillonite, was obtained from Inner Mongolia, China. Its cation exchange capacity (CEC) is 108.4 mmol/100 g bentonite. The bentonite sample was pulverized and filtered through a 100-mesh sieve.

Ag_3PO_4-Ben was prepared by cationic exchange and phosphate acid reaction. The preparation procedure is shown in Fig. 1. First, Tollens' reagent was prepared. A few drops of diluted sodium hydroxide were added to 1 mmol/L silver nitrate solution. In this solution, Ag^+ ions from the aqueous silver nitrate were hydrated as $[Ag(H_2O)_2]^+$ complexes, that is, diaquasilver (I) ions. Dihydroxyargentate (I) complexes are not stable and are immediately dehydrated to produce silver oxide (Ag_2O). The solid part was separated and washed with deionized water. Aqueous ammonia was then added to a conical flask that contained the washed silver oxide until the brown silver oxide dissolved. Silver ions existed as $[Ag(NH_3)_2]^+$ complexes in the mixture.

The $[Ag(NH_3)_2]^+$ complexes were then dropped into the bentonite suspension with stirring at 300 rpm. The total amount of silver ions dropped was equal to the bentonite CEC. After stirring for 2 h, the suspension was water-bathed at 80 °C for 12 h. The solid part was separated and washed several times with deionized water. In this step, $[Ag(NH_3)_2]^+$ replaced Ca^{2+} in the bentonite and then converted to Ag_2O in the bentonite inter-layer.

Finally, H_3PO_4 was dropped into the modified bentonite suspension. The reaction $Ag_2O + H_3PO_4 \rightarrow Ag_3PO_4 + H_2O$ occurred in the bentonite and Ag_3PO_4 particles formed between the lamellar layers. $[Ag(NH_3)_2]^+$ specifically served as the intermediate medium to yield the Ag_3PO_4 crystal.

2.2. Characterization

X-ray diffraction (XRD) patterns of the prepared samples were determined using an X-ray diffractometer (Max-2550PC, Rigaku D) with a Cu K_α radiation (40 kV, 300 mA) at 0.154 nm to confirm the structure of the materials. All XRD patterns were obtained from 0.5° to 80° with a scan speed of 4°/min. The elemental composition was detected by X-ray photoelectron spectroscopy (XPS, Amicus, Shimadzu Co., Japan). Fourier transform infrared (FTIR) spectra were obtained using the KBr pressed disk technique on a Thermo Nicolet Nexus 670 FTIR spectrophotometer. The FTIR spectra in the range of 4000–400 cm^{-1} were recorded with a resolution of 4 cm^{-1}, and 64 interferograms were collected. Ultraviolet–vis (UV–vis) diffusion reflectance spectra were recorded using a UV-vis spectrometer (UV-2450, Shimadzu) and converted to absorption spectra by the standard Kubelka–Munk method. Specific surface areas of the prepared photocatalysts were measured using the Brunauer, Emmett, and Teller (BET) method (Autosorb-iQ2-MP, Quantachrome Instruments). X-ray fluorescence (XRF, Horiba XGT-1000WR) was used to determine the silver content in the products.

2.3. Photocatalytic degradation of aqueous Orange II solutions

The activities of the samples were evaluated by the photocatalytic decomposition of Orange II. A mixture of Orange II solutions (70 mg/L, 500 mL) and the given photocatalyst (Ag_3PO_4-Ben or Ag_3PO_4) was magnetically stirred in the absence of light for 60 min to ensure adsorption-desorption equilibrium between the photocatalyst and Orange II. The weights of the solid powder (Ag_3PO_4-Ben and Ag_3PO_4) are both 200 mg/L. The mixture was then stirred under visible light irradiation using a 300 W Xe arc lamp or

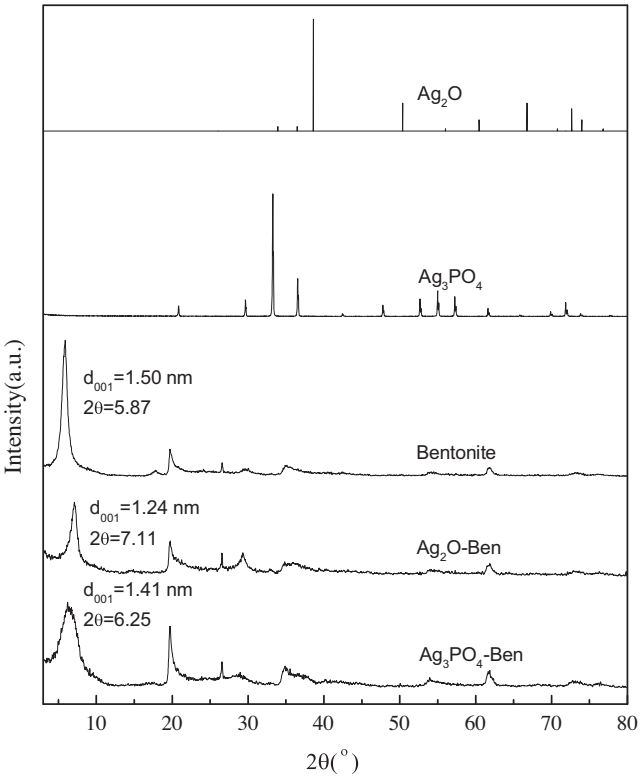

Fig. 2. X-ray diffraction patterns of bentonite, Ag_2O, Ag_3PO_4, Ag_2O-Ben, and Ag_3PO_4-Ben.

nature sunlight at about 900–1000 lux (tested by a Digital Lux meter TES-1339, Shanghai, China). At given time intervals, 5 mL of the suspension was collected and centrifuged to remove photocatalyst particles. The UV–vis adsorption spectrum of the centrifuged solution was recorded using a UV-vis spectrophotometer (UV-2450, Shimadzu, Japan) to determine the conversion of the reaction.

The processes for evaluation of the stability and recyclability of the composites were conducted as follows: at the end of each cycle, the suspension was centrifuged and the supernatant was analyzed and discarded. The dose of the Ag_3PO_4-Ben and Ag_3PO_4 were 400 mg/L and 200 mg/L, respectively. When H_2O_2 was added, the H_2O_2 (30%) amount was 60 μL per liter of Orange II solution.

3. Results and discussion

3.1. XRD spectra

XRD Analysis can be used to determine the layer distances of clay, which is a powerful piece of information that helps to clarify the microscopic status of the intercalated molecules in the clay structure. Clay minerals are known to vary their interlayer distances depending on the nature of the intercalated molecules. XRD measurements were carried out on the present samples, and typical XRD profiles are shown in Fig. 2 for natural bentonite, Ag_2O, Ag_3PO_4, Ag_2O-Ben, and Ag_3PO_4-Ben. The layer distances, as varied by the intercalation of Ag_2O and Ag_3PO_4, were estimated from the position of the (0 0 1) diffraction peak. The XRD pattern of natural bentonite exhibited typical reflections of montmorillonite with a series of narrow and sharp peaks that indicate a high degree of crystallinity [15]. The (0 0 1) peak appeared at 5.87° (2θ), from which the inter-lamellar distance was found to be 1.50 nm. The $d_{0\,0\,1}$ of Ag_2O-Ben was 1.24 nm, as determined by the peak appearing at 7.11° (2θ). After reaction with H_3PO_4, the Ag_3PO_4-Ben composite was formed and the distance of the d_{001} became 1.41 nm. The peak of Ag_3PO_4-Ben became broader and less intense after pillaring with Ag compounds, indicating that the layered periodic structure was slightly damaged. This damage was confirmed by the disappearance of the bentonite subprime diffraction of (0 0 3) at 5.87° (2θ). The results thus prove that the substance in the inter-lamella changed.

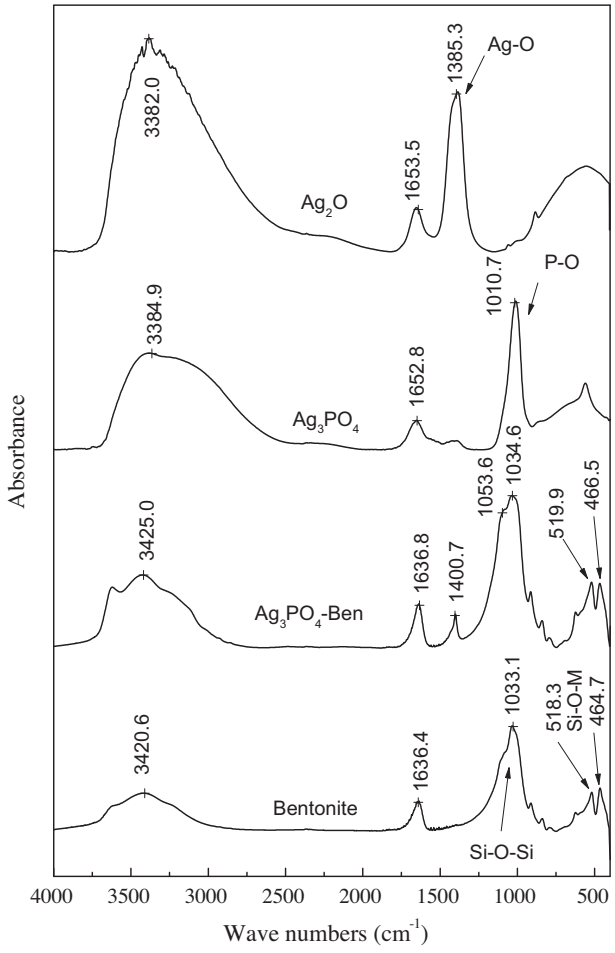

Fig. 3. FTIR spectra of raw bentonite, Ag_3PO_4-Ben, Ag_3PO_4, and Ag_2O.

An excess distance or "clearance space" can be defined as the value obtained by subtraction of the intrinsic layer thickness (0.96 nm) from the observed layer distance [16]. The observed layer distance for Ag_3PO_4-Ben (1.41 nm) subtracts the thickness of silicate-aluminum-hydroxide layer is about 0.45 nm. The clearance space depends on the volume of intercalation molecules. It could be inferred that the particle size of Ag_3PO_4 is not larger than 0.45 nm.

For free Ag_3PO_4 and Ag_2O particles, all the diffraction peaks are well indexed as diffraction peaks of cubic Ag_3PO_4 and Ag_2O (JCPDS No. 06-0505 and No. 76-1393, respectively). However, not all of the peaks of Ag_3PO_4-Ben could be indexed to the cubic structure of Ag_3PO_4, which may be due to the presence of extremely fine Ag_3PO_4 particles with only one or two unit cells (smaller than 0.45 nm) that have insufficient periodicity for XRD detection.

3.2. FTIR spectra, XRF and XPS analysis

In Fig. 3, the FTIR spectra of raw bentonite, Ag_3PO_4-Ben, Ag_3PO_4, and Ag_2O were recorded from 400 cm^{-1} to 4000 cm^{-1} and compared with one another.

Absorption peaks from 3400 cm^{-1} to 3650 cm^{-1} are due to the H—O—H stretching vibrations of water molecules and to –OH stretching vibrations of adsorbed water. The bands at 1630 cm^{-1}

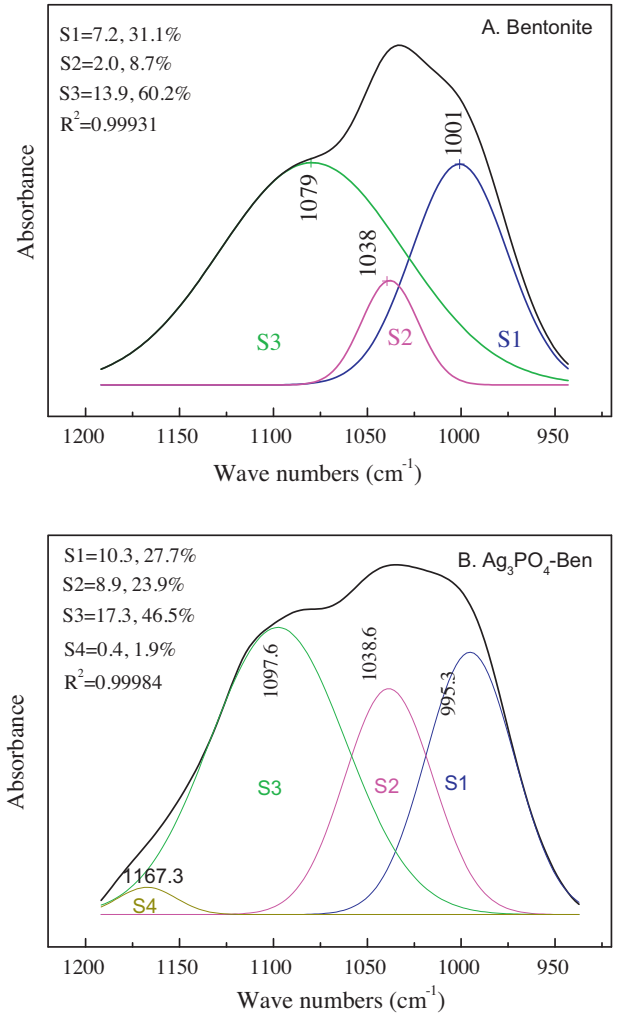

Fig. 4. Fitting of bentonite and Ag_3PO_4-Ben I.R. bands (900–1200 cm^{-1}) by Gaussian curves.

and 1650 cm^{-1} are related to H_2O bending modes. Strong bands for raw bentonite from 1030 cm^{-1} to 1035 cm^{-1} are related to the stretching vibrations of Si—O—Si bonds, which are characteristic of phyllosilicate minerals.

Bentonite characteristic bands for Si—O—Si bonding (1030–1035 cm^{-1}) remained the same after loading with Ag_3PO_4 and Ag_2O. Adsorption bands near 1010 cm^{-1} are assigned to P—O^- groups, which comprise the phosphate non-bridging oxygen portion of PO_4 tetrahedra in a chain structure [17,18]. The Si—O—Si and P—O adsorption bands overlapped each other, and a broad shoulder peak appeared at 1053.6 cm^{-1}.

The broad infrared bands of the Si—O—Si groups (900–1200 cm^{-1}) of bentonite and Ag_3PO_4-Ben were fitted using Gaussian distribution. The FTIR spectra of overlapped peaks were resolved into separate bands (Fig. 4). The absorbance areas of bentonite could obviously be fitted to S1, S2, and S3, while the absorbance areas of Ag_3PO_4-Ben could be fitted to S1, S2, S3, and S4, with a correlation coefficient R^2 of over 0.999 for both compounds. The percentage of the absorbance area of S2 with a peak at 1038 cm^{-1} increased from 8.7% to 23.9%, thus confirming the presence of the P—O group with absorbance at 1010 cm^{-1}.

The strong absorbance of Ag_2O at 1385.3 cm^{-1} was due to the bond-stretching vibrations of Ag—O. This adsorption peak also appeared in Ag_3PO_4-Ben but was shifted to 1400.7 cm^{-1}.

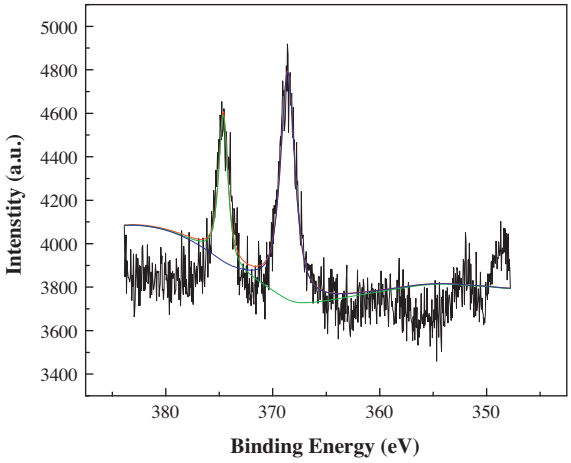

Fig. 5. The XPS spectra of Ag_3PO_4-Ben particles (Ag 3d).

The chemical compositions of natural bentonite and Ag_3PO_4-Ben were determined by XRF analysis, and the results showed that aluminum silicate was the prevalent component of natural bentonite. Calcium was the third component in quantity, while metals such as Fe, Mg, and Na were present in trace amounts. After pillaring by Ag_3PO_4, a silver content of 10.72 wt% was found. The results confirmed that Ag_3PO_4 existed in the inter-lamellar layers despite the fact that no Ag peak was reflected in the XRD pattern.

The XPS was carried out to investigate the surface compositions and chemical state of Ag_3PO_4-Ben particles (Fig. 5). The binding energies obtained from the XPS analysis were corrected by referencing C_{1s} to 284.8 eV. The Ag_{3d} spectra of Ag_3PO_4 was composed of two individual peaks at ~374 and ~368 eV, which could be attributed to Ag $3d_{3/2}$ and Ag $3d_{5/2}$ binding energies, respectively [19]. The presence of Ag species existed as Ag^+ was confirmed.

3.3. UV–vis diffuse reflectance spectrum

The optical absorption property is a key factor to consider when selecting a photocatalyst. Fig. 6 shows the UV–vis absorption spectra of Ag_3PO_4, Ag_3PO_4-Ben and bentonite. It can be clearly seen that the bare Ag_3PO_4 can absorb solar energy with a wavelength shorter than ~530 nm as reported by Yi et al. [1]. Bentonite shows little adsorption in the range of visible light. However, with the load of Ag_3PO_4, the Ag_3PO_4-Ben exhibited the absorption in a wavelength range shorter 503 nm. Compared with the bare Ag_3PO_4, the absorption intensity slightly decreases for the low content of Ag_3PO_4 in

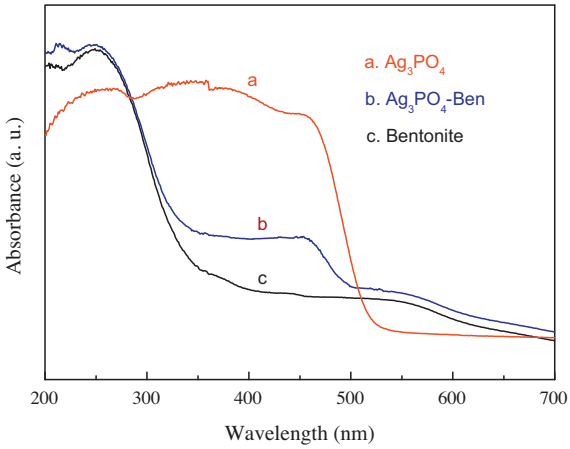

Fig. 6. UV–vis adsorption spectra of Ag_3PO_4, bentonite and Ag_3PO_4-Ben.

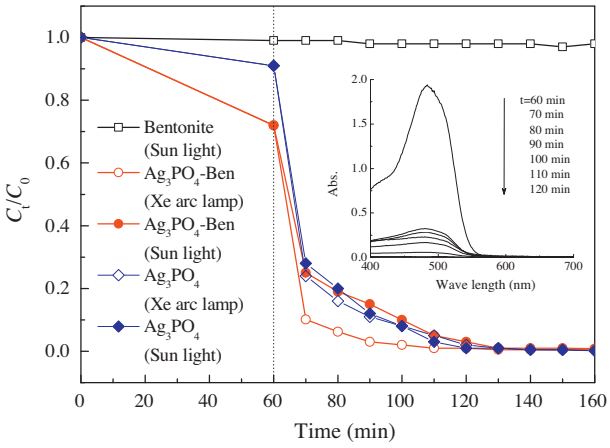

Fig. 7. Photocatalytic degradation of Orange II solution (70 mg/L, 500 mL) by Ag_3PO_4 and Ag_3PO_4-Ben with/without H_2O_2 under Xe light or sunlight.

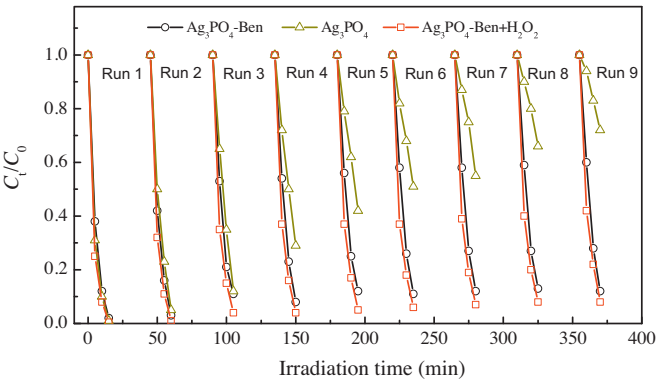

Fig. 8. Repeated photocatalytic degradation of Orange II solution under Xe arc lamp irradiation (Ag_3PO_4-Ben: 400 mg/L; Ag_3PO_4: 200 mg/L; Ag_3PO_4-Ben + H_2O_2: 400 mg/L; 60 μL/L 30% H_2O_2; Orange II solution: 500 mL with a concentration of 70 mg/L).

the composite. This result indicates that Ag_3PO_4-Ben is a potential photocatalyst for sunlight-driven applications.

3.4. Photocatalytic performance

The photocatalytic property of the composite was evaluated in terms of the decolorization of Orange II under Xe arc lamp and sunlight irradiation (Fig. 7).

During the adsorption process, only 9% of the Orange II was adsorbed on bare Ag_3PO_4 while 28% of the Orange II was adsorbed on Ag_3PO_4-Ben, which can be mainly attributed to the large specific surface area of Ag_3PO_4-Ben (170 m^2/g). The specific surface area of Ag_3PO_4-Ben was much higher than those of Ag_3PO_4 and bentonite (36.5 and 56.3 m^2/g, respectively).

Compared with the raw bentonite, the adsorption capacities on Ag_3PO_4-Ben greatly improved not only because of the specific surface area, but the special structure of bentonite. Bentonite has a layered structure, which makes large interlayer space. Bentonite has permanent negative charge due to the isomorphous substitution of Al^{3+} for Si^{4+} in the tetrahedral layer and Mg^{2+} for Al^{3+} in the octahedral layer. This negative charge is balanced by the presence of exchangeable cations (Na^+, Ca^{2+}, etc.) in the lattice structure, which make it perform well in sorption of cationic dyes by cationic exchange mechanism [8,9,20]. However, it fails in sorption of anionic dyes because of the negative charge on the edge of the bentonite sheet [21,22]. Orange II is a kind of anionic dye with a sulfonate ion in its molecular structure. The repellant of the negative charges between orange II and the bentonite particle decreased the adsorption capacity [23].

During the synthesis of Ag_3PO_4-Ben the negative charge was neutralized and the specific surface areas increased. Besides the specific surface areas, the special structure is also an important part for the adsorption by modified bentonite. Hydration of the bentonite allows water to migrate to the interlayer which forces the platelets apart and causes the inter-layers to widen. In the aqua, the bentonite swelled and the much more inner surface exposed which lead to the increase in the adsorption. Heterogeneous photocatalytic degradation generally occurs after the reactant is adsorbed on the surface of the catalyst, so adsorption is actually a pre-step for the consequent photocatalytic reaction [24]. While bentonite does not possess any photocatalytic property, its high adsorption capacity evidently improves degradation.

Under sunlight exposure, the degradation rates of Orange II with Ag_3PO_4-Ben or free Ag_3PO_4 were both high at 90% for 90 min. From 60 min to 70 min, the C_t/C_0 of Ag_3PO_4-Ben decreased from 0.72 to 0.25, 47% of the dye was degraded. And under the same condition, 63% of the dye was degraded by Ag_3PO_4 particles. The results clearly show that the bentonite supported Ag_3PO_4 can be applied for the degradation under sunlight.

The degradation of the solution catalyzed by Ag_3PO_4-Ben under the Xe arc lamp was approximately 99% within 90 min, including an adsorption period of 60 min. The decrease in absorption peaks of Orange II at λ_{max} = 478 nm indicate that the double bond of nitrogen-to-nitrogen was destroyed. Under the Xe arc lamp light, the C_t/C_0 of Ag_3PO_4-Ben decreased from 0.72 to 0.10, 62% of the dye was degraded. At the same condition, 67% of the dye was degraded by Ag_3PO_4. The results show that at the same illumination energy, the Ag_3PO_4 particles are more active than Ag_3PO_4-Ben. One of the reasons of the lower active for Ag_3PO_4-Ben is the strong adsorption of bentonite carrier. When too much Orange II molecules were adhere to the inner site of bentonite, some of the light rays were blocked by the dye molecules and the activity of Ag_3PO_4-Ben was decreased. The other reason is lower Ag available, which seems the major contribution for lower activity, although Bentonite helps for adsorption.

The silver content was only 10.72 wt% in Ag_3PO_4-Ben but 77.3 wt% for Ag_3PO_4; that is to say that the possible available quantity of Ag in Ag_3PO_4-Ben catalyst was 10.72% × 200 mg = 21.44 mg, and that in Ag_3PO_4 catalysts was 77.3% × 200 mg = 154.6 mg. So the activity of Ag_3PO_4-Ben was about 5.67 times higher than Ag_3PO_4 for this photocatalytic process [(62%/21.44)/(67%/154.6) = 6.67 times]. That means, silver, a noble metal, may be saved by the incorporation of bentonite, the cost of the treatment greatly decreased.

3.5. Evaluation of the stability and recyclability of the composites

Stability and recyclability of a catalyst are important issues related to their practical use. When Ag_3PO_4 is used as a photocatalyst without a sacrificial reagent, it can photo-corrode and decompose to weakly active Ag during O_2 evolution from water. Its photocatalytic activity then gradually deteriorates, which is the main hindrance for the practical application of Ag_3PO_4 as a recyclable and highly efficient photocatalyst [1]. The recyclability of Ag_3PO_4 and Ag_3PO_4-Ben were compared in 9 runs. Wang et al. [25] proposed a facile wet chemical-oxidation method to rejuvenate Ag_3PO_4 from weak Ag as a recyclable and highly efficient photocatalyst. The effect of H_2O_2 on rejuvenation was also evaluated as shown in Fig. 8.

The degradation rates of Orange II as catalyzed by Ag_3PO_4 and Ag_3PO_4-Ben were both high in the first run and the rate of Ag_3PO_4 was a little higher than that of Ag_3PO_4-Ben. However, from the second run, the rate catalyzed by Ag_3PO_4 slightly decreased and got even worse than that of Ag_3PO_4-Ben. Finally, at the last run of the

recycle, the catalyst (Ag_3PO_4) almost lost its activity, which might be explained by silver reduction. Silver captures excited electrons and is consequently reduced on the surface of the catalyst in metallic form. Ultimately, all the Ag_3PO_4 nanoparticles decomposed to Ag. The redox potential of the Ag^+/Ag pair is 0.80 V, whereas at the presence of excessive of PO_4^{3-} ions, the redox potential of Ag species decreases markedly to 0.45 V (Ag_3PO_4/Ag) [1,26].

The bentonite-loaded Ag_3PO_4 (Ag_3PO_4-Ben) showed much higher removal efficiency and stability than free Ag_3PO_4 particles because that silver reduction was minimal during light irradiation. This improvement may have resulted from the special structure of bentonite. Bentonite is a silicate, which is an extremely flat crystal flake that carries a relatively strong net-negative ionic charge. The negative charge is compensated for by adsorbing a cation between lamellar layers. In this study, the exchangeable Ca^{2+} was replaced by Ag^+, which is oxidized to Ag_2O and then reacts with H_3PO_4 to yield Ag_3PO_4 salt deposited in the inter-layers. Other compensated cations (e.g., H^+) remain in the inter-layers to maintain the neutral charge of the particle. Cations can easily capture excited electrons that inhibit the reduction of silver.

With the support of bentonite, Ag_3PO_4 in the interlayer also can be rejuvenated by H_2O_2. Upon addition of H_2O_2, Ag is oxidized under a PO_4^{3-} atmosphere to became a recyclable and highly efficient photocatalyst [25]. However, compared with the system without any H_2O_2 added, the efficiency increased little.

Natural bentonite has almost no catalytic activity, but it is relatively easy to convert them into useful catalysts by either acid treatment or cation exchange with other metal ions [27]. Clay catalysts have been shown to contain both Brønsted and Lewis acid sites [28]. The silver ion exchanged and phosphoric acid treated bentonite can be simply regarded as solid acids and act as heterogeneous catalysts, which greatly improved the stability and photocatalytic activity.

There are some researches on improvement of the photocatalyst activities of Ag_3PO_4 by immobilization it on some supports such as flaky layered double hydroxides [4], TiO_2[6], AgCl [29], carbon quantum dots [30], and SnO_2 [31]. These methods improved the activities of Ag_3PO_4 to varying levels; however, few of these researches investigated the recycle of the catalysis. Bentonite improved the stability of the catalysis for its special layered structure and the microenvironment around the active catalyst.

4. Conclusion

In this study, a novel method for intercalation silver salt into bentonite interlayers is described. As a result, the very fine Ag_3PO_4 crystalline grains (less than 0.45 nm) were obtained in the interlayers of bentonite (Ag_3PO_4-Ben). Ag_3PO_4-Ben particles exhibited high catalytic efficiency for Orange II degradation under visible light irradiation. The degradation of the solution catalyzed by Ag_3PO_4-Ben under the Xe arc lamp was approximately 99% within 90 min, including an adsorption period of 60 min. Also the stability was greatly improved with the support of bentonite. After the 9 runs of the recycle, Ag_3PO_4-Ben almost kept the same activity with the removal efficiency of 90%. The special structure of bentonite and the microenvironment around the catalysis enhanced the stability. In addition, the silver content in the photocatalyst composite decreased from 77.3 wt% in bare Ag_3PO_4 to 10.7 wt% in the Ag_3PO_4-Ben composite. The low Ag content significantly reduces the cost of Ag_3PO_4-based photocatalysts. This facile process for the preparation of Ag_3PO_4-Ben composites can be adopted for the synthesis of other bentonite-supported silver salt-based catalysts, such as AgCl-Ben and AgBr-Ben and other salts.

Acknowledgments

This work was supported by the National Natural Science Foundation of China (Grant Nos. 21007005 and 20907038), the Project Funded by the Priority Academic Program Development of Jiangsu Higher Education Institutions and Technology Innovation Team of Colleges, and the Universities-Funded Project of Jiangsu Province (No. 2011-24).

References

[1] Z. Yi, J. Ye, N. Kikugawa, T. Kako, S. Ouyang, H. Stuart-Williams, H. Yang, J. Cao, W. Luo, Z. Li, Y. Liu, R.L. Withers, Nature Materials 9 (2010) 559–564.
[2] C.T. Dinh, T.D. Nguyen, F. Kleitz, T.O. Do, Chemical Communications 47 (2011) 7797–7799.
[3] Y. Bi, H. Hu, S. Ouyang, G. Lu, J. Cao, J. Ye, Chemical Communications 48 (2012) 3748–3750.
[4] X. Cui, Y. Li, Q. Zhang, H. Wang, International Journal of Photoenergy 2012 (2012) 1–6.
[5] M. Ge, N. Zhu, Y. Zhao, J. Li, L. Liu, Industrial and Engineering Chemistry Research 51 (2012) 5167–5173.
[6] W. Yao, B. Zhang, C. Huang, C. Ma, X. Song, Q. Xu, Journal of Materials Chemistry 22 (2012) 4050.
[7] P.V. Kamat, Chemical Reviews 93 (1993) 267–300.
[8] Q.H. Hu, S.Z. Qiao, F. Haghseresht, M.A. Wilson, G.Q. Lu, Industrial and Engineering Chemistry Research 45 (2006) 733–738.
[9] S.S. Tahir, N. Rauf, Chemosphere 63 (2006) 1842–1848.
[10] J. Hefne, W. Mekhemer, N. Alandis, O. Aldayel, T. Alajyan, J. King, Journal of King Abdulaziz University Science 22 (2010) 155–176.
[11] J.X. Chen, L.Z. Zhu, Catalysis Today 126 (2007) 463–470.
[12] J.X. Chen, L.Z. Zhu, Journal of Hazardous Materials 185 (2011) 1477–1481.
[13] S.A. Khan, R. Riazur, M.A. Khan, Waste Management 15 (1995) 271–282.
[14] U. Zafar, I. Khan, F. Jamshed, S. Naeem, Journal of the Chemical Society of Pakistan 24 (2002) 92–97.
[15] R.L. Zhu, T. Wang, J.X. Zhu, F. Ge, P. Yuan, H.P. He, Chemical Engineering Journal 160 (2010) 220–225.
[16] A. Habti, D. Keravis, P. Levitz, H. van Damme, Journal of the Chemical Society, Faraday Transactions 2 (80) (1984) 67–83.
[17] P.Y. Shih, Materials Chemistry and Physics 84 (2004) 151–156.
[18] Y. Arai, D.L. Sparks, Journal of Colloid and Interface Science 241 (2001) 317–326.
[19] H. Zhang, G. Wang, D. Chen, X. Lv, J. Li, Chemistry of Materials 20 (2008) 6543–6549.
[20] C.C. Wang, L.C. Juang, T.C. Hsu, C.K. Lee, J.F. Lee, F.C. Huang, Journal of Colloid and Interface Science 273 (2004) 80–86.
[21] P. Baskaralingam, M. Pulikesi, D. Elango, V. Ramamurthi, S. Sivanesan, Journal of Hazardous Materials 128 (2006) 138–144.
[22] G. Crini, Bioresource Technology 97 (2006) 1061–1085.
[23] J.F. Ma, B.Y. Cui, J.A. Dai, D.L. Li, Journal of Hazardous Materials 186 (2011) 1758–1765.
[24] R.W. Matthews, Journal of Catalysis 113 (1988) 549–555.
[25] H. Wang, Y. Bai, J. Yang, X. Lang, J. Li, L. Guo, Chemical European Journal 18 (2012) 5524–5529.
[26] Y. Bi, J. Ye, Chemical Communications (2009) 6551–6553.
[27] F. Tomul, Chemical Engineering Journal 185 (2012) 380–390.
[28] W.T. Wang, H.Z. Liu, T.B. Wu, P. Zhang, G.D. Ding, S.G. Liang, T. Jiang, B.X. Han, Journal of Molecular Catalysis A Chemical 355 (2012) 174–179.
[29] Y. Bi, S. Ouyang, J. Cao, J. Ye, Physical Chemistry Chemical Physics 13 (2011) 10071.
[30] H. Zhang, H. Huang, H. Ming, H. Li, L. Zhang, Y. Liu, Z. Kang, Journal of Materials Chemistry 22 (2012) 10501–10506.
[31] L. Zhang, H. Zhang, H. Huang, Y. Liu, Z. Kang, New Journal of Chemistry 36 (2012) 1541–1544.